Journal of Materials Chemistry

Cite this: DOI: 10.1039/c1jm12767e

www.rsc.org/materials

PAPER

Porous manganese oxide generated from lithiation/delithiation with improved electrochemical oxidation for supercapacitors†

Hui Xia,*[a] Ying Shirley Meng,[b] Xiaogan Li,[c] Guoliang Yuan[a] and Chong Cui[a]

Received 16th June 2011, Accepted 3rd August 2011
DOI: 10.1039/c1jm12767e

For manganese oxides with low manganese oxidation states, such as MnO or Mn_3O_4, the electrochemical oxidation during potential cycling is critical to achieve high supercapacitor performance. In this work, dense Mn_3O_4 thin films are prepared by pulsed laser deposition. An electrochemical lithiation/delithiation process is applied to the Mn_3O_4 thin film, which leads to a nanoporous structure of the film and greatly increases the porosity of the film. The nanoporous MnO_x thin film electrode exhibits significantly improved supercapacitive performance compared to the as-prepared Mn_3O_4 thin film electrode. After 1000 cyclic voltammetric scans in 1 M Na_2SO_4 electrolyte between 0 and 1 V, only part of the surface of the as-prepared Mn_3O_4 thin film transforms into a MnO_2 porous structure while the complete film of the nanoporous MnO_x transforms into a MnO_2 porous structure. It is believed that the nanoporous structure, which facilitates the electrolyte penetration, leads to the completion of electrochemical oxidation through the film during the potential cycling, resulting in promising supercapacitive performance of the film.

Introduction

As alternative energy storage devices, supercapacitors have gained increasing attention due to their higher specific power and longer cycle life compared to rechargeable batteries, and higher specific energy compared to conventional capacitors.[1,2] Due to the high power feature, supercapacitors can be used as complementary power devices to rechargeable batteries in various applications, such as hybrid electric vehicles, mass rapid transit, power tools *etc.*, that require high/peak power pulses for time-dependent usage. According to their different energy storage mechanisms, supercapacitors can be divided into electric double layer capacitors (EDLCs) using electrostatic charge separation and pseudocapacitors based on fast superficial redox reactions.[3] Among various electrode materials, transitional metal oxides are redox-active materials and very high specific capacitance has been reported for ruthenium dioxide.[4] However, the high cost and toxic nature of ruthenium dioxide limit its commercial application. Therefore, other transition metal oxides with lower cost, such as NiO, Fe_2O_3, SnO_2, MnO_2, have attracted considerable attention with the anticipation that they will replace ruthenium dioxide as low-cost and green electrode materials.[5–8]

In searching for alternative electrode materials, MnO_2 has been extensively investigated due to its excellent reversibility and acceptable specific capacitance.[9,10] However, the supercapacitive performance of MnO_2 is correlated with its crystallographic structure and specific surface area.[11] As the pseudocapacitance comes from the reversible redox transitions of electrochemical active materials, a high specific capacitance can only be achieved when the crystal structure of MnO_2 can provide favorable pathways for intercalation and deintercalation of protons or alkali metal cations. Since the fast, faradic redox reactions occur at the electrode surface, increasing the specific surface area of MnO_2 can increase the utilization of the electrode material, thus leading to a high specific capacitance. Various methods have been developed to synthesize nanostructured MnO_2 with desired crystal structure including sol–gel method, precipitation, electrochemical deposition, chemical bath deposition, electrostatic spray deposition, and hydrothermal synthesis.[12–15] When Mn has a lower oxidation state (<4+), the corresponding oxides such as MnO, Mn_3O_4 and Mn_2O_3 do not show a promising capacitive behavior. However, it was found in many recent papers that MnO_x ($x < 2$) with a lower oxidation state can be electrochemically oxidized to MnO_2 during the potential cycling in an aqueous Na_2SO_4 electrolyte.[16–18] During the oxidation process, water incorporation into the MnO_2 and a porous structure formation are observed, which greatly improves the capacitive

[a]*School of Materials Science and Engineering, Nanjing University of Science and Technology, Xiaolingwei 200, Nanjing, Jiangsu, 210094, P. R. China. E-mail: jasonxiahui@gmail.com; Fax: +86 25 8431 5159; Tel: +86 25 8431 5606*
[b]*Department of Nano Engineering, University of California San Diego, La Jolla, California, 92093-0448, USA*
[c]*School of Electronic Science and Technology, Dalian University of Technology, Dalian, Liaoning, 116024, P. R. China*

† Electronic supplementary information (ESI) available: 3 cycles charge/discharge curves of a Mn_3O_4 thin film for the lithiation/delithiation process, cross-section FESEM image of a Mn_3O_4 thin film deposited on a Si substrate, AFM image of a MnO_x thin film, high magnification FESEM image of a Mn_3O_4 thin film and a MnO_x thin film. See DOI: 10.1039/c1jm12767e

performance of the as-prepared MnO_x.[17] Therefore, electrochemical oxidation could be an effective method to synthesize nanostructured and hydrated MnO_2 with promising capacitive performance for supercapacitors. However, the correlation between the as-prepared microstructure of MnO_x and the electrochemical oxidation process is still not clear. Djurfors *et al.* reported that a Mn/MnO thin film electrode can be prepared by physical vapor deposition and it exhibits promising capacitive behavior after the electrochemical oxidation.[18] However, their study indicates that only the surface of the film can be transformed into a porous hydrated layer with a thick dense bottom layer unchanged.[18]

It is speculated that the specific capacitance of the MnO_x electrode depends on how much of the electrode material can be oxidized to MnO_2. The porosity of the electrode material prior to the electrochemical oxidation could be an important factor influencing the electrochemical oxidation process. In this work, dense Mn_3O_4 thin film electrodes are prepared by pulsed laser deposition. By using electrochemical lithiation/delithiation, a nanoporous structure of the film is formed. The electrochemical oxidation and supercapacitor performance of the dense film and the nanoporous film are studied. The relationship between the microstructure of the MnO_x thin film and the electrochemical oxidation process is discussed.

Experimental

Preparation of Mn_3O_4 thin film and nanoporous MnO_x thin film

Mn_3O_4 thin films were deposited on the stainless steel (SS) substrates by pulsed laser deposition (PLD) using a metallic Mn target. A Lambda Physik KrF excimer laser with wavelength 248 nm was used in the deposition. The film was deposited at a substrate temperature of 600 °C with an oxygen partial pressure of 200 mTorr. To perform the electrochemical lithiation/delithiation, a lab-made Swagelok cell was assembled with a Mn_3O_4 thin film as the working electrode, a Li foil as both counter and reference electrode and 1 M $LiPF_6$ in EC/DEC (1 : 1, vol%) as the electrolyte. The cell was charged and discharged between 0.01 and 3 V at a current density of 50 μ A cm^{-2} for 3 cycles (Fig. S1, ESI†). After the electrochemical lithiation/delithiation, the cell was disassembled and the prepared MnO_x thin film electrode was rinsed with deionized water, and then dried for further characterization.

Materials characterization

The crystallographic information of the thin films was investigated using powder X-ray diffraction (XRD, Shimadzu X-ray diffractometer 6000, Cu-Kα radiation). Morphologies of the Mn_3O_4 thin film sample, the MnO_x thin film sample, and sample after electrochemical oxidation were characterized by field emission scanning electron microscopy (FESEM, Hitachi S4300). The morphology and structure of thin films were further investigated by transmission electron microscopy (TEM) and high resolution transmission electron microscopy (HRTEM, JEOL, JEM-2010). The oxidation states of Mn for the MnO_x thin film before and after the electrochemical oxidation were investigated by X-ray photoelectron spectroscopy (XPS, PHI Quantera SXM Scanning X-ray Microprobe).

Electrochemical measurements

All electrochemical measurements were conducted using a Solartron 1287 electrochemical interface combined with a Solartron 1260 frequency response analyzer. For the supercapacitive performance measurements, a three-electrode cell system composed of a thin film as the working electrode, a high surface carbon rod as the counter electrode, and an Ag/AgCl reference electrode was employed. The capacitive behavior of both the Mn_3O_4 thin film electrode and the MnO_x thin film electrode were characterized by cyclic voltammetry (CV) in 1 M Na_2SO_4 electrolyte at room temperature. CV measurements were performed on the three-electrode cells in the voltage window between 0 and 1.0 V at a scan rate of 50 mV s^{-1}. The electrochemical oxidation of the Mn_3O_4 thin film or the MnO_x thin film occurs at the high potential during the CV scans. Electrochemical impedance spectra (EIS) of different thin film electrodes were measured at the open-circuit potential with an AC amplitude of 10 mV in the frequency range from 100 kHz to 100 mHz.

Results and discussion

Fig. 1 shows the XRD patterns of the Mn_3O_4 film prepared by PLD and the MnO_x film after the electrochemical lithiation/delithiation. The XRD pattern of the as-prepared Mn_3O_4 thin film (Fig. 1b) is in good agreement with that of the tetragonal hausmannite Mn_3O_4 structure (JCPDS card no. 24-0734). The diffraction peaks from the Mn_3O_4 film can be indexed as (101), (112), (103), (211), (004), and (224). After electrochemical lithiation/delithiation, the XRD pattern of the MnO_x film shows no diffraction peak from the film. It is probable that the diffraction peaks of the MnO_x thin film are too weak to be observed due to the strong and sharp diffraction peaks of the SS substrate. The difference in the XRD patterns between the as-prepared Mn_3O_4 thin film and the MnO_x film indicates that there is significant structure change induced in the Mn_3O_4 thin film during the lithiation/delithiation process.

The FESEM images with different magnifications of the as-prepared Mn_3O_4 thin film and the MnO_x thin film after electrochemical lithiation/delithiation are shown in Fig. 2. As shown in Fig. 2a, the surface of the as-prepared Mn_3O_4 thin film appears compact and the film is closely packed with well-defined grains. The grain size ranges from several tens to several hundreds of

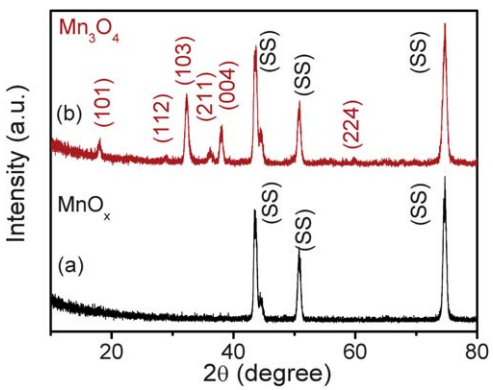

Fig. 1 XRD patterns for the as-prepared Mn_3O_4 thin film and nanoporous MnO_x thin film.

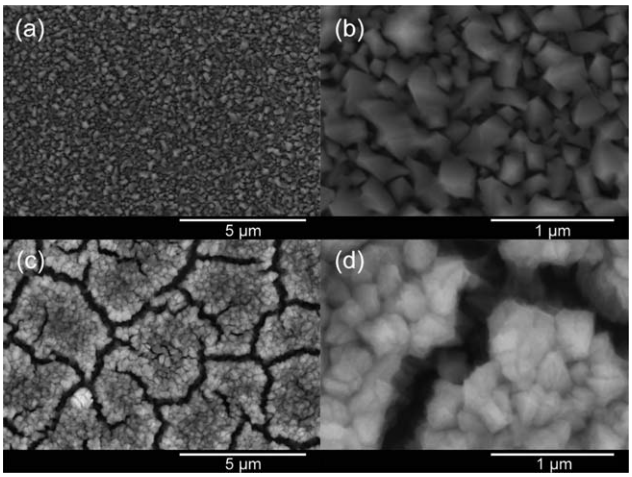

Fig. 2 (a) and (b) FESEM images for the as-prepared Mn_3O_4 thin film. (c) and (d) FESEM images for the nanoporous MnO_x thin film after lithiation/delithiation.

nanometres (Fig. 2b). Thin film thickness is estimated to be about 300 nm from a cross-section FESEM image of a Mn_3O_4 thin film deposited on a Si substrate (Fig. S2, ESI†). As shown in Fig. 2c, cracks with different sizes and lengths form in the MnO_x film after the electrochemical lithiation/delithiation. The lithiation/delithiation of Mn_3O_4 thin film is accompanied with large volume expansion/contraction, which induces huge strain in the film and finally leads to crack formation. Despite the formation of cracks, no peeling of the film is observed, indicating that good adhesion between the film and the substrate is retained after lithiation/delithiation. The grains of the MnO_x film seem to retain their original shape as in the as-prepared Mn_3O_4 thin film. However, the surface of the grain of the MnO_x film is not as smooth as that of the as-prepared Mn_3O_4 thin film, indicating changes inside the grains (also see AFM image in Fig. S3, ESI†).

To further investigate the microstructure change of the Mn_3O_4 film before and after the lithiation/delithiation, part of the film was scratched by a blade for TEM characterization. TEM images of the as-prepared Mn_3O_4 thin film and the MnO_x thin film are shown in Fig. 3. A TEM image of several clustered grains from the as-prepared Mn_3O_4 thin film is given in Fig. 3a. The grains appear very compact without any porosity. The electron diffraction pattern (ED) of a single grain demonstrates the single-crystalline nature of Mn_3O_4 as shown in Fig. 3b. The well-resolved lattice spacings of about 4.85 and 3.17 Å from the ED pattern correspond to the value of (101) and (112) planes of tetragonal Mn_3O_4, which are in agreement with the XRD result. In contrast to the intact single crystal grains, the grains after lithiation/delithiation are pulverized with a high porosity as shown in Fig. 3c and 3d. The HRTEM in Fig. 3e demonstrates the formation of disordered nanograins and nanopores of less than 10 nm in the original single crystal grain. The lattice fringes in Fig. 3f clearly confirm the crystallinity of the nanograins. The inter-planar space measured as 0.23 nm can be attributed to the (200) plane of the MnO crystal structure. The ED pattern inserted in Fig. 3f indicates that the original single crystalline grain becomes polycrystalline after lithiation/delithiation. Furthermore, instead of Mn_3O_4, the ED pattern can be indexed as the MnO phase. It is speculated that there is some irreversible

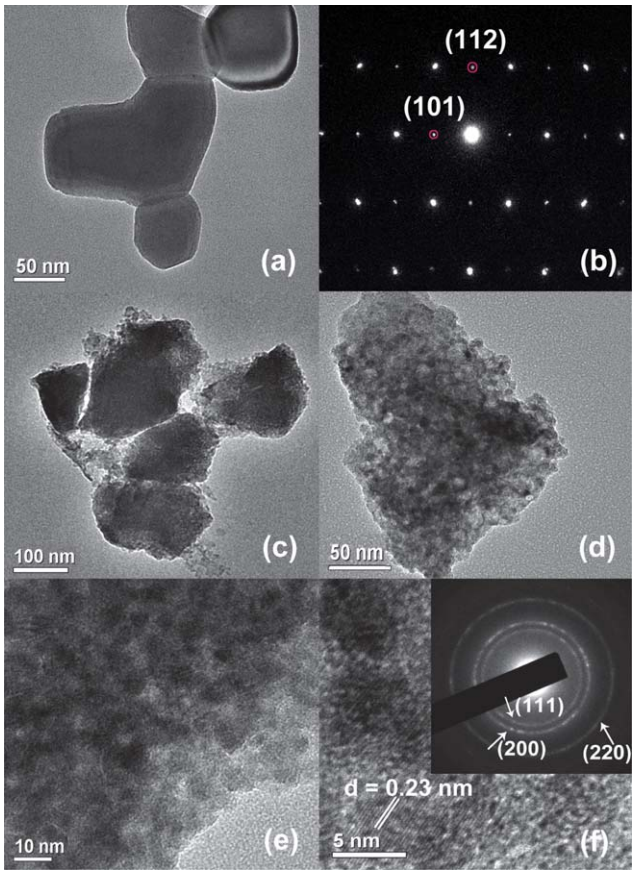

Fig. 3 (a) TEM image of the as-prepared Mn_3O_4 thin film sample. (b) ED pattern of the as-prepared Mn_3O_4 thin film sample. (c) and (d) TEM images of the nanoporous MnO_x thin film sample. (e) and (f) HRTEM images of the nanoporous MnO_x thin film sample (inset in (f) is the ED pattern of the nanoporous MnO_x thin film sample).

capacity between the lithiation and delithiation (Fig. S1, ESI†), which means not all the Li inserted in the as-prepared Mn_3O_4 film is removed after the delithiation. Due to incomplete Li removal, the Mn metal may not be completely oxidized to Mn_3O_4 but to MnO, which is in good agreement with Fang *et al.*'s result.[19] Due to some residual Li in the film, the formula MnO_x is used to denote the film after lithiation/delithiation for convenience.

To investigate the electrochemical oxidation and capacitive performance of the as-prepared Mn_3O_4 and nanoporous MnO_x thin film electrodes, 1000 CV potential scans between 0 and 1 V at a scan rate of 50 mV s^{-1} were performed on both electrodes. Fig. 4a shows the CV curves for the first cycle and the 1000th cycle for the Mn_3O_4 thin film electrode. For the first cycle, the CV curve exhibits an obvious current leap near the upper potential limit, which could be attributed to the electrochemical oxidation process and/or water decomposition with oxygen evolution. According to Broughton and Brett *et al.*, Mn could be electrochemically oxidized to Mn^{2+}, Mn_3O_4, Mn_2O_3 and MnO_2 with increasing anodic potential in the sodium sulfate aqueous solution, and the onset of MnO_2 exists in the potential at 0.8 V (*vs.* Ag/AgCl) in 1 M sodium sulfate aqueous solution.[20] The initial specific capacitance of the film is only 12.3 F g^{-1}, which is contributed to by the Mn_3O_4 phase. As the potential scan

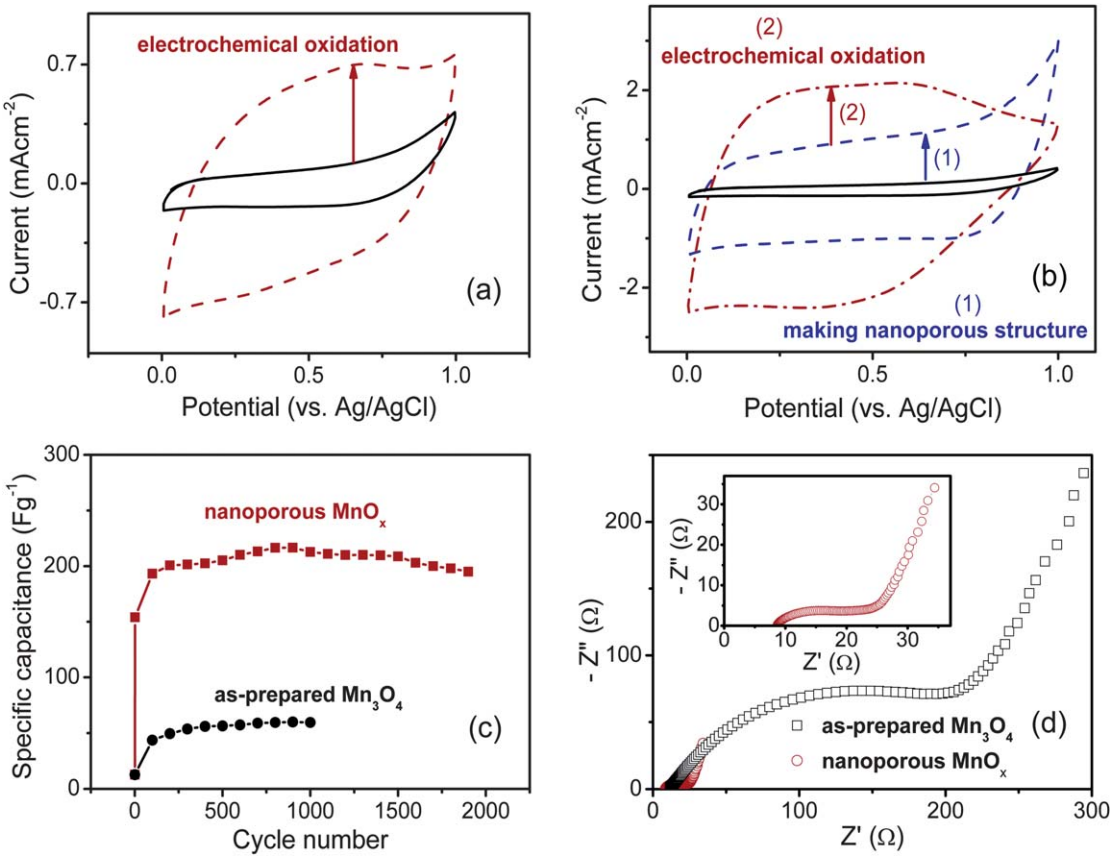

Fig. 4 (a) The first and the 1000th cycle CV curves of the as-prepared Mn_3O_4 thin film. (b) The first cycle CV curve of the as-prepared Mn_3O_4 thin film, the first and 1000th cycle CV curves of the nanoporous MnO_x thin film. (c) The specific capacitance of the as-prepared Mn_3O_4 and the nanoporous MnO_x as a function of cycle number. (d) Nyquist plots of the as-prepared Mn_3O_4 and the nanoporous MnO_x thin films.

continues, the current density of the CV curve keeps increasing and becomes stabilized after about 1000 cycles. At the 1000th cycle, the specific capacitance of the film is increased to 57.6 F g^{-1} with a larger area of the CV curve. The CV curve at the 1000th cycle exhibits a distorted rectangular shape without an obvious current leap at the upper potential limit, indicating the electrochemical oxidation process is completed. Fig. 4b shows the CV curves for the first cycle of the as-prepared Mn_3O_4 thin film, the first cycle and the 1000th cycle of the nanoporous MnO_x thin film electrodes, respectively. For the first cycle, the CV curve of the nanoporous MnO_x thin film exhibits a much larger area compared to that of the Mn_3O_4 thin film, indicating significantly improved capacitive performance for the Mn_3O_4 thin film after lithiation/delithiation. The specific capacitance of the thin film electrode is increased to 150 F g^{-1} after the lithiation/delithiation. This could be explained by the nanoporous structure of the film, which leads to a much larger surface area of the film. An obvious current leap at the upper potential limit can be observed from the first cycle CV curve of the nanoporous MnO_x thin film electrode, which indicates an obvious electrochemical oxidation process. As shown in Fig. 4b, after 1000 potential scan cycles, the current leap at the upper potential limit disappears, indicating that the electrochemical oxidation process is completed and the water decomposition at high potential could be neglected for this electrode. The current density of the CV curve of the nanoporous MnO_x thin film electrode keeps increasing during the continuous potential scan and reaches a maximum after 1000 cycles. After 1000 cycles, the final specific capacitance of the nanoporous MnO_x thin film electrode reaches about 213 F g^{-1}, which is much larger than that of the Mn_3O_4 thin film electrode. The specific capacitance as a function of cycle number for the as-prepared Mn_3O_4 thin film electrode and the nanoporous MnO_x thin film electrode are compared in Fig. 4c. It seems that the lithiation/delithiation process plays an important role in improving the specific capacitance of the thin film electrode. Without such a process, the final specific capacitance of the thin film electrode can only reach one fourth of that of the nanoporous MnO_x thin film electrode. For the nanoporous thin film electrode, the specific capacitance increases significantly in the first 100 cycles and then increases slowly up to the 1000th cycle. The specific capacitance reaches a maximum at about the 1000th cycle and starts to decrease slowly after 1000 cycles. After 2000 cycles, the thin film electrode still can deliver a specific capacitance of about 193 F g^{-1}, which is 91% of the specific capacitance at the 1000th cycle.

Nyquist plots for the as-prepared Mn_3O_4 thin film electrode and the nanoporous MnO_x thin film electrode are shown in Fig. 4d. For both Nyquist plots, a semicircle in the high-frequency region and a straight line at low frequency region can be observed. The diameter of the semicircle in the high-frequency region corresponds to the charge transfer resistance at the electrode/electrolyte interface. It is clear to see that the

charge-transfer resistance of the thin film electrode reduces remarkably after the electrochemical lithiation/delithiation. The small charge-transfer resistance of the nanoporous MnO_x thin film electrode is due to the formation of a nanoporous structure, which facilitates the penetration of the electrolyte into the electrode and greatly increases the interface between the electrode and electrolyte. For a simple electrode–electrolyte system, the low frequency straight line should exhibit a slope of 45° if the process is under diffusion control, or a slope of 90° if the system is purely capacitive in nature. The finite slope of the straight line represents the diffusive resistance of the electrolyte in the electrode pores and cation diffusion in the host materials. It can be seen that the slope of the straight line for the nanoporous MnO_x thin film electrode is larger than that of the as-prepared Mn_3O_4 thin film electrode, indicating a lower diffusive resistance of the electrolyte for the MnO_x thin film electrode. It is believed that the numerous nanopores in the MnO_x thin film electrode facilitate the penetration of the electrolyte into the electrode, leading to fast diffusion of the electrolyte into the pores of the MnO_x thin film electrode.

To investigate the surface morphology evolution induced by the electrochemical oxidation and the difference of capacitive behavior between the as-prepared Mn_3O_4 thin film electrode and the nanoporous MnO_x thin film electrode, we performed FESEM measurements on the two thin film electrodes after 1000 CV potential scans. FESEM images of the as-prepared Mn_3O_4 thin film electrode and the nanoporous MnO_x thin film electrode after potential scans are given in Fig. 5a and 5b. After potential scans, part of the surface of the Mn_3O_4 thin film is transformed into a porous structure. However, underneath the porous layer, most of the film retains its original morphology before potential scans, indicating the electrochemical oxidization only occurs at part of the surface of the film (Fig. S4(a), ESI†) In comparison, the nanoporous MnO_x film is fully transformed into a highly porous structure after the potential scans (Fig. S4(b), ESI†), indicating that the electrochemical oxidization occurs everywhere in the nanoporous film. To investigate the porous structure of the film after the electrochemical oxidation, part of the nanoporous MnO_x film after potential scans was scratched to do the TEM measurement. As shown in Fig. 5c, it can be seen that the film after the electrochemical oxidation is composed of interconnected nanosheets. The film after the electrochemical oxidation exhibits a nearly amorphous structure as confirmed by the inserted ED pattern in Fig. 5c. Djurfors and Broughton *et al.* reported that a porous, amorphous, and hydrated MnO_2 layer can form at the surface of a Mn/MnO film after the electrochemical oxidation.[18] Xie *et al.* and Lokhande *et al.* reported that Mn_3O_4 thin films can transform into birnessite-type MnO_2 thin films after the electrochemical oxidation.[16,17] To confirm the Mn is oxidized to a high valence state after the electrochemical oxidation, XPS measurements on the nanoporous MnO_x film and the film after 1000 CV potential scans were carried out. Fig. 5d shows the Mn 2p XPS spectra for the two thin film samples. The peak attributed to Mn 2p3/2 shifts from 654.6 to 642.1 eV, which indicates the oxidation process from Mn^{2+} to Mn^{4+} and formation of MnO_2 after the CV potential scans.[21–23]

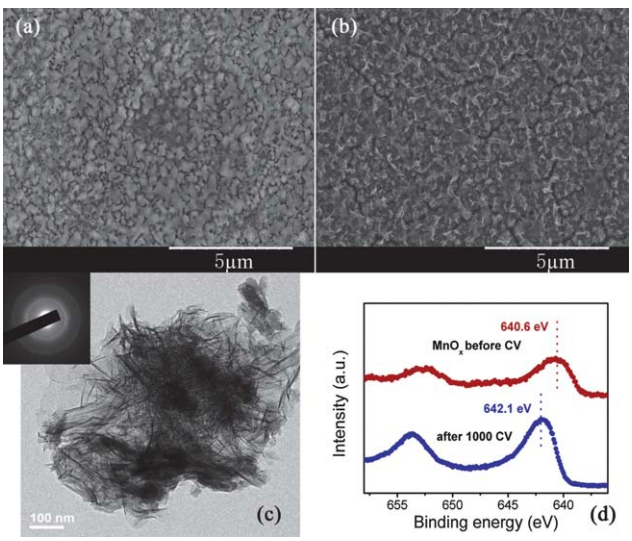

Fig. 5 (a) FESEM image of the as-prepared Mn_3O_4 thin film after 1000 CV potential cycles. (b) FESEM image of the nanoporous MnO_x thin film after 1000 CV potential cycles. (c) TEM image of the nanoporous MnO_x thin film sample after 1000 CV potential cycles. (d) Mn 2p spectra of the nanoporous MnO_x thin film sample before and after 1000 CV potential cycles.

The electrochemical oxidation process is critical to the capacitive performance for the series of manganese oxides with low manganese oxidation states (<4+). MnO_x ($x < 2$) usually exhibits poor capacitive performance and can not be used as promising electrode materials for supercapacitors. However, after the electrochemical oxidation, not only can Mn be oxidized to 4+, as MnO_2 is a promising electrode material for supercapacitor, but also a porous structure is formed *in situ*, which can further improve the capacitive performance. Therefore, maximizing the specific capacitance of the electrode material depends on the degree of completion of the electrochemical oxidation of the electrode material. Djurfors *et al.* found that the electrochemical oxidation can only form a porous layer on top of a dense Mn/MnO film and they believed that the porous layer is solely responsible for the capacitive behavior of the film.[20] If the initial film is dense and thick, only the surface area can be transformed into MnO_2 with a porous structure, resulting in a low utilization of the film and low specific capacitance. In the present study, it is found that the porosity of the initial film before the electrochemical oxidation is critical to the electrochemical oxidation process. The electrochemical oxidation processes of the as-prepared Mn_3O_4 thin film and nanoporous MnO_x thin film are illustrated in Fig. 6. For the as-prepared Mn_3O_4 thin film, the film is composed of closely packed single crystal grains and only the surface area of the film can be exposed to the electrolyte. Since the grains are closely packed and single crystal in nature, it is difficult for the electrolyte to diffuse into the electrode, resulting in limited electrode/electrolyte interface. The potential scans between 0 and 1 V in Na_2SO_4 electrolyte are also associated with Na^+ adsorption/desorption at the film surface and Na^+ intercalation/deintercalation into/from the film. These electrochemical processes cannot induce significant volume change or structure change of the film to create pores or cracks in the film. During the electrochemical oxidation process, the oxidation of Mn can only occur at the electrode/electrolyte interface. Without extra pores for the penetration of electrolyte, the electrochemical oxidation process will stop till a porous layer

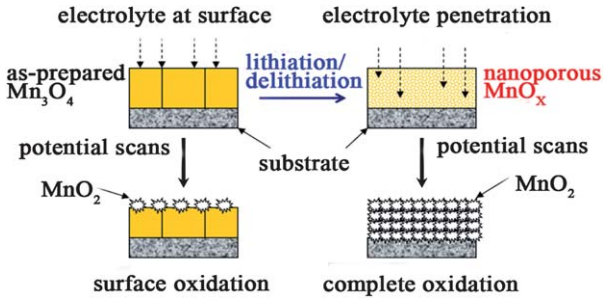

Fig. 6 Schematic illustration of the electrochemical oxidation processes of the as-prepared Mn_3O_4 thin film and the nanoporous MnO_x thin film.

forms at the surface. For the nanoporous MnO_x thin film, the film is composed of nanograins and nanopores less than 10 nm. During the lithiation/delithiation process, the film is under high strain due to the large volume change, which finally leads to crack formation. At the same time, the original single crystal Mn_3O_4 grains are all pulverized, resulting in the nanoporous structure with a high porosity. All these cracks and nanopores formed during the lithiation/delithiation process can facilitate the electrolyte penetration into the film, enabling the lithiation/delithiation process to proceed from the top to the bottom of the film. In this case, the electrolyte can penetrate into the electrode through the numerous pores, which greatly increases the electrode/electrolyte interface. With the nanoporous structure, the electrochemical oxidation process can occur anywhere in the electrode, leading to oxidation of the whole film and complete transformation of the film into the final porous structure composed of MnO_2 nanosheets. The completion degree of electrochemical oxidation of the film is critical to the capacitive performance of the final product. After electrochemical oxidation, the nanoporous MnO_x film delivers a specific capacitance 4 times higher than that of the as-prepared Mn_3O_4 film. Therefore, the porosity of the initial electrode is important for the completion degree of the electrochemical oxidation and the final specific capacitance of the electrode.

Conclusions

The lithiation/delithiation method has been successfully employed to form a nanoporous structure *in situ* from the dense Mn_3O_4 thin film prepared by PLD. The electrochemical oxidation occurs on both the as-prepared Mn_3O_4 thin film electrode and the nanoporous MnO_x thin film electrode during the CV potential scans, which leads to improvement of the capacitive performance. However, the final specific capacitance of the nanoporous MnO_x thin film electrode after electrochemical oxidation is four times higher than that of the as-prepared Mn_3O_4 thin film electrode. It was found that the electrochemical oxidation only occurs at the surface of the as-prepared Mn_3O_4 thin film while it take place throughout the nanoporous film. It is believed that the porosity of the initial film plays an important role in the electrochemical oxidation process. The numerous nanopores in the MnO_x film serve as diffusion channels, facilitating the penetration of the electrolyte and leading to the completion of electrochemical oxidation through the film. The specific capacitance of the electrode is correlated to the completion degree of electrochemical oxidation of the electrode.

Acknowledgements

This research is supported by Nanjing University of Science and Technology through the research grant NUST Research Funding (AB41385, 2010ZDJH07 and AB41358).

Notes and references

1 C. Z. Yuan, B. Gao, L. F. Shen, S. D. Yang, L. Hao, X. J. Lu, F. Zhang, L. J. Zhang and X. G. Zhang, *Nanoscale*, 2011, **3**, 529.
2 S. Chen, J. W. Zhu and X. Wang, *ACS Nano*, 2010, **4**, 6212.
3 P. Simon and Y. Gogotsi, *Nat. Mater.*, 2008, **7**, 845.
4 T. S. Hyun, H. L. Tuller, D. Y. Youn, H. G. Kim and I. D. Kim, *J. Mater. Chem.*, 2010, **20**, 9172.
5 Y. Wang, C. Y. Foo, T. K. Hoo, N. Ng and J. Y. Lin, *Chem.–Eur. J.*, 2010, **16**, 3598.
6 T. Zhu, J. S. Chen and X. W. Lou, *J. Mater. Chem.*, 2010, **20**, 7015.
7 Y. F. Yuan, X. H. Xia, J. B. Wu, J. L. Yang, Y. B. Chen and S. Y. Guo, *Electrochim. Acta*, 2011, **56**, 2627.
8 J. A. Yan, E. Khoo, A. Sumboja and P. S. Lee, *ACS Nano*, 2010, **4**, 4247.
9 J. M. Wang, E. Khoo, J. Ma and P. S. Lee, *Chem. Commun.*, 2010, **46**, 2468.
10 J. T. Zhang, J. W. Jiang and X. S. Zhao, *J. Phys. Chem. C*, 2011, **115**, 6448.
11 N. Munichandraiah and S. J. Devaraj, *J. Phys. Chem. C*, 2008, **112**, 4406.
12 C. K. Lin, K. H. Chuang, C. Y. Lin, C. Y. Tsay and C. Y. Chen, *Surf. Coat. Technol.*, 2007, **202**, 1272.
13 H. Xia, J. K. Feng, H. L. Wang, M. O. Lai and L. Lu, *J. Power Sources*, 2010, **195**, 4410.
14 J. Y. Luo and Y. Y. Xia, *J. Electrochem. Soc.*, 2007, **154**, A987.
15 M. Xu, L. Kong, W. Zhou and H. Li, *J. Phys. Chem. C*, 2007, **111**, 19141.
16 D. P. Dubal, D. S. Dhawale, R. R. Salunkhe and C. D. Lokhande, *J. Electroanal. Chem.*, 2010, **647**, 60.
17 Y. Dai, K. Wang and J. Y. Xie, *Appl. Phys. Lett.*, 2007, **90**, 104102.
18 B. Djurfors, J. N. Broughton, M. J. Brett and D. G. Ivey, *Acta Mater.*, 2005, **53**, 957.
19 X. P. Fang, X. W. Guo, Y. Mao, Y. S. Hu, J. Z. Wang, Z. X. Wang, F. Wu, H. K. Liu and L. Q. Chen, *Electrochem. Commun.*, 2010, **12**, 1520.
20 B. Djurfors, J. N. Broughton, M. J. Brett and D. G. Ivey, *J. Electrochem. Soc.*, 2006, **153**, A64.
21 G. A. Rizzi, R. Zanoni, S. Di Siro, L. Peeriello and G. Granozzi, *Surf. Sci.*, 2000, **462**, 187.
22 A. Moses Ezhil Raj, S. Grace Victoria, V. Bena Jothy, C. Ravidhas, J. Wollschlager, M. Suendorf, M. Neumann, M. Jayachandran and C. Sanjeeviraja, *Appl. Surf. Sci.*, 2010, **256**, 2920.
23 D. P. Dubal, D. S. Dhawale, R. R. Salunkhe and C. D. Lokhande, *J. Electroanal. Chem.*, 2010, **647**, 60.